Surface Electromyography-Based Analysis of the Lower Limb Muscle Network and Muscle Synergies at Various Gait Speeds

Tie Liang, Huacong Miao, Hongrui Wang, Xiaoguang Liu, and Xiuling Liu

***Abstract*— Gait movement is an important activity in daily human life. The coordination of gait movement is directly affected by the cooperation and functional connectivity between muscles. However, the mechanisms of muscle operation at different gait speeds remain unclear. Therefore, this study addressed the gait speed effect on the changes in cooperative modules and functional connectivity between muscles. To this end, surface electromyography (sEMG) signals were collected from eight key lower extremity muscles of twelve healthy subjects walking on a treadmill at high, middle, and low motion speeds. Nonnegative matrix factorization (NNMF) was applied to the sEMG envelope and intermuscular coherence matrix, yielding five muscle synergies. Muscle functional networks were constructed by decomposing the intermuscular coherence matrix, revealing different layers of functional muscle networks across frequencies. In addition, the coupling strength between cooperative muscles grew with gait speed. Different coordination patterns among muscles with changes in gait speed related to the neuromuscular system regulation were identified.**

***Index Terms*— Muscle network, sEMG, gait speed, muscle synergies.**

I. Introduction

AS ONE of the most fundamental activities in daily life, gait movement has been studied based on different gait speeds in several fields, such as kinetics, where peak kinematic and kinetic parameters were predicted based on gait speed (velocity) [1]. For example, neuroscience uses it to predict the decline in attention and psychomotor speed in older adults based on gait speed [2]. In clinical medicine, gait speed is used to predict mortality and major morbidity in patients after cardiac surgery [3]. The field of kinesiology also studies the effect of different gait speeds on human stability during gait. With the development of noninvasive acquisition technology, surface electromyography (sEMG) detection methods have been widely used, and analyzing gait at different speeds based on sEMG signals has become a new research hotspot.

Since sEMG signals can directly reflect muscle activation, many previous studies have been conducted mainly by quantifying the differences in sEMG signal characteristics at different gait speeds. Thus, Schlink et al. investigated the spatial entropy and center of gravity of sEMG signals based on different gait velocities and found that sEMG signal amplitudes were spatially inhomogeneous at higher gait speeds [4]. Hof et al. reported that the mean sEMG changed predictably with increasing gait speed [5]. The relationship between isolated muscles and gait speed has also been studied. McCain et al. demonstrated the relationship between the electromyographic activity of the soleus muscle and walking speed regulation [6]. Byrne et al. revealed the effect of speed variation in walking on the sEMG of the anterior tibialis muscle under healthy gait conditions [7]. However, gait movement results from the interplay of many muscles in the lower extremities, and a single muscle activation pattern failed to reflect the intermuscular relationships fully.

Gait movement is a very complex control task involving multi-muscle coordination. Increases or decreases in speed can affect muscle coordination patterns during gait progression [8]. Several studies have confirmed that the musculoskeletal and nervous systems could build motor modules by coactivating muscle groups, i.e., muscle synergy, simplifying the control of multiple muscles by the nervous system [9]. On the other hand, the common modulation of the sEMG envelope is thought to be muscle-synergistic. It has been shown to reveal the synchronous activation of synergistic muscle groups and thus control the mechanism of human motor action generation [10]. Recently, muscle synergy analyses have been used to elaborate alterations in the neuromuscular system. Three to

Manuscript received 30 October 2022; revised 16 January 2023; accepted 31 January 2023. Date of publication 6 February 2023; date of current version 14 February 2023. This work was supported in part by the National Key Research and Development Program of China under Grant 2017YFB1401200; in part by the National Natural Science Foundation of China under Grant U20A20224; in part by the Natural Science Foundation of Hebei Province under Grant F2020201048, Grant F2021201002, and Grant F2021201005; and in part by the Key Project of Hebei Province Department of Education under Grant ZD2020146. *(Corresponding authors: Xiaoguang Liu; Xiuling Liu.)*

This work involved human subjects or animals in its research. Approval of all ethical and experimental procedures and protocols was granted by the Ethics Review Committee of the Affiliated Hospital of Hebei University.

The authors are with the Key Laboratory of Digital Medical Engineering of Hebei Province, College of Electronic Information Engineering, Hebei University, Baoding, Hebei 071002, China (e-mail: hbuliangtie@163.com; 20217018080@stumail.hbu.edu.cn; hongrui@hbu.edu.cn; lxg_hbu@163.com; liuxiuling@hbu.edu.cn).

Digital Object Identifier 10.1109/TNSRE.2023.3242911

five groups of muscle synergies have been identified by studying lower limb muscle synergies in gait movements [11]. Some researchers have applied muscle synergy analysis to subjects with poststroke injuries. Thus, Pan et al. studied changes in muscle synergy during arm extension in stroke patients [12]. By comparing muscle synergy in stroke patients and healthy individuals, Clark et al. showed that stroke patients required fewer muscle synergy modules [13].

Functional muscle network analysis quantifies the functional connectivity between motor-related muscles. It can identify the frequency characteristics of specific muscles modulated by common neural inputs, quantified by intermuscular coherence decomposition to determine shared frequencies at which particular muscles are comodulated by common neural inputs. Recently, muscle network-based analysis methods have been applied to study the movement of different populations. Neurophysiological signals such as sEMG generally exhibit oscillatory and synchronous characteristics, making them well suited for frequency-domain analysis [14], [15]. Coherence is a classical frequency-domain method for the coupling analysis of paired neurophysiological signals, which measures the linear relationship between two signals by normalized cross-spectrum [16], [17], [18]. In recent years, coherence method has been effectively applied to quantify the strength of intermuscular connections in muscle networks. Kerkmen et al. used the coherence approach to map functional muscle networks to study interactions between the central nervous system and the musculoskeletal system [19]. Houston et al. observed significant changes in the alpha (8-13 Hz) band of the upper limb muscle network in patients with chronic stroke based on coherence analysis [20]. These studies indicated that muscle network analysis based on coherence analysis is expected to be an effective tool for exploring the mechanism of multi-muscle interaction during voluntary movement.

In recent years, more and more researchers have applied the graph theory approach to neuroscience. Xu et al. explored and compared the functional connectivity between motor execution and motor imagery using graph theory [21]. Piovanelli et al. simplified the estimation of muscle activation pattern using graph theory [22]. Xi et al. applied graph theory to establish an effective cortical-muscle network and investigated the regulatory mechanisms of the cortical-muscular system during the development of muscle fatigue [23]. These studies demonstrate that the differences in muscle coordination patterns under different tasks can be effectively visualized and characterized by the sEMG-based graph theory analysis methods. Therefore, muscle network analysis based on graph theory may become an effective method for analyzing gait movements at different speeds.

This paper analyzes the synergy between lower limb muscles at different gait speeds, constructs a functional muscle network based on quantifying the intermuscular coherence, and then explores the muscle network differences at different motion speeds based on graph theory. Functional muscle networks demonstrate connectivity between muscle groups from different frequency ranges. Few studies have focused on muscle synergy and functional muscle networks in lower limb muscles under different gait speed conditions, which limits understanding of the lower-limb neuromuscular control mechanisms. To fill this gap, we analyze both muscle synergy and functional muscle networks to verify the control mode of the central nervous system and identify the intrinsic association of intermuscular synergy and coupling. With a new perspective of exploring the mechanisms of muscle synergy at different gait speeds, this study is expected to provide a comparative benchmark for studying gait in patients with various neuromuscular dysfunctions or injuries.

II. Materials and Methods

A. Subjects

Twelve healthy right-foot dominant male subjects were recruited for this study (23.5 $\pm$ 1.1 years of age; weight: 71.4 $\pm$ 7.9 kg; height: 173.7 $\pm$ 5.3 cm). All the subjects signed written informed consent forms before the experiment. This study was officially approved by the Ethics Review Committee of the Affiliated Hospital of Hebei University (HDFY-LL-2020-091).

B. Experimental Procedure

All subjects were asked to perform gait movements on a treadmill at different speeds (low, medium, and high), corresponding to the treadmill speeds of 4, 8, and 12 km/h, respectively. The sEMG data for each set of experiments with at least 30 steps were recorded, after which the subjects were allowed to rest, avoiding the muscle fatigue effect.

C. Data Acquisition

The sEMG data of eight muscles, namely rectus femoris (RF), vastus medialis (VM), vastus lateralis (VL), semitendinosus (ST), biceps femoris (BF), tibialis anterior (TA), gastrocnemius (GM), and soleus (SO) were acquired from the right lower limbs of all subjects via a Noraxon wireless sEMG acquisition system (Noraxon, USA), as shown in Fig. 1. These data were sampled at 1500 Hz after online bandpass filtering between 5 and 450 Hz.

D. Data Analysis

Muscle synergy identifies coactive muscle groups in motor task performance by decomposing sEMG-sEMG amplitudes. Functional muscle networks were determined by decomposing sEMG-sEMG coherence to identify shared frequencies at which specific muscles were co-modulated by common neural inputs.

To analyze the muscle synergy, the sEMG signal was high-pass filtered (with a cutoff frequency of 20 Hz) and subsequently rectified using the Hilbert transform. The rectified sEMG signal identified the sEMG envelope by low-pass filtering (with a cutoff frequency of 10 Hz). Nonnegative matrix decomposition using the sEMG envelope was applied to extract muscle synergies [9], [24]. The sEMG envelope was decomposed into two nonnegative matrices, one of which reflected the synergistic effect and the other reflected the corresponding activation pattern [25]. The variance-accounted-for (VAF) was used to determine the number of synergistic muscle modules.

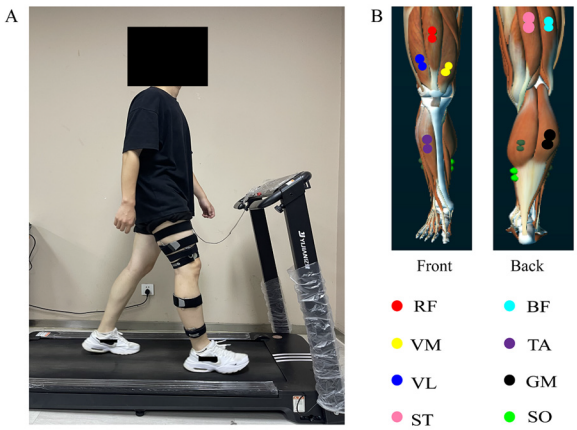

Fig. 1. Experimental setting. (A) sEMG was collected by the subject on the treadmill. (B) The position of the muscles collected by sEMG. Colored dots denote sEMG placements at leg muscles: RF (red), VM (yellow), VL (blue), ST (pink), BF (cyan), TA (purple), GM (black) and SO (green).

The amplitude squared coherence estimates are a function of frequency with values between 0 and 1. These values indicate the degree of correspondence at each frequency. The amplitude squared coherence is a function of the power spectral density, applying a Hanning window of 500 ms length with a 50% window overlap and calculating the intermuscular coherence at a spectral resolution of 2 Hz over the frequency range of 0-50 Hz, using the following equation:

$$C_{\mathrm{xy}}(f) = \frac{\left|P_{\mathrm{xy}}(f)\right|^2}{P_{xx}(f)\ P_{yy}(f)} \tag{1}$$

where C_{xy} is the coherence between the sEMG signals x and y, f is the frequency, P_{xx} and P_{yy} are the self-spectra of signals x and y, respectively, while P_{xy} is the mutual spectrum of signals x and y.

The coherence matrix A was constructed by intermuscular coherence. The nonnegative matrix decomposition of alternating least squares was applied to the coherence matrix to decompose it into several different frequency component matrices (W) and their corresponding coupling intensity matrices (H) as follows:

$$A_{f*m} \approx W_{f*n} * H_{n*m} + E_{f*m} \tag{2}$$

where f is the frequency, n is the number of frequency components, and m is the number of muscle pairs. Since parameter n was unknown before the analysis, the VAF was used to determine the number of synergistic muscle modules. Considering the threshold of 90% of VAF [26], it was calculated via the error matrix E and the Frobenius norms of the coherence matrix A as:

$$VAF = 1 - \frac{|E|^2_{fro}}{|A|^2_{fro}} \tag{3}$$

To visualize the functional muscle networks, a threshold value of 30% of the maximum edge weight of a single adjacency matrix is selected, the network topology is drawn using a uniform threshold value for each group, and the edges in the network topology are defined as low connection strength (0-33%), medium connection strength (34-66%), and high connection strength (67-100%) according to the relationship between the individual edge weights and the maximum edge weights. The thickness of the connection lines in the functional muscle network topology diagram describes the connection strength between muscles; if the coupling strength between muscles is stronger, the connection lines are thicker, and if the coupling strength between muscles is weaker, the connection lines are thinner.

Three network metrics were calculated to evaluate the topological characteristics of individual functional muscle networks: global efficiency, clustering coefficients, and mediator centrality [27]. The average shortest path length between all pairs of network nodes is the network's characteristic path length [28]. The global efficiency is inversely proportional to the feature path length. A higher global efficiency value indicates a complete network function. The following formula was used to calculate the global efficiency:

$$E = \frac{1}{n}\sum_{i\in N} E_i = \frac{1}{n}\sum_{i\in N}\frac{\sum_{j\in N, j\neq i} d_{ij}^{-1}}{n-1} \tag{4}$$

where E_i is the efficiency of node i, N is the set of all nodes in the network, d_{ij} is the shortest path length (distance), between nodes i and j, and n is the number of nodes. The clustering coefficient describes the degree to which the nodes in a graph cluster together into clusters. Specifically, it is the degree to which the neighbors of a point are connected. The average clustering coefficient measures how well a network is clustered as a whole [29]. The clustering coefficient can be derived as follows:

$$C = \frac{1}{n}\sum_{i\in N} C_i = \frac{1}{n}\sum_{i\in N}\frac{2t_i}{k_i(k_i-1)} \tag{5}$$

where C_i is the clustering coefficient of node i ($C_i = 0$ for $k_i < 2$), t_i is the number of triangles around node i, k_i is the degree of node i. Betweenness centrality is defined as the number of times a given node is passed by the shortest path in the network, reflecting the role and influence of the corresponding node or edge in the whole network, corresponding to the hub point or intermediary point. The formula for calculating the medial centrality is as follows:

$$b_i = \frac{1}{(n-1)(n-2)}\sum_{\substack{h,j\in N\\ h\neq j, h\neq i, j\neq i}}\frac{\rho_{hj}(i)}{\rho_{hj}} \tag{6}$$

where b_i is the betweenness centrality of node i, where ρ_{hj} is the number of shortest paths between h and j, and $\rho_{hj}\ (i)$ is the number of shortest paths between h and j that pass through node i. where the clustering coefficients and betweenness centrality are averaged across nodes to obtain a global metric of the network. All three network metrics were calculated based on the weighted adjacency matrix.

Differences between network metrics at each layer of the coherent network were analyzed using the univariate analysis of variance (ANOVA), with experimental conditions at different speeds as factors and network metrics as dependent

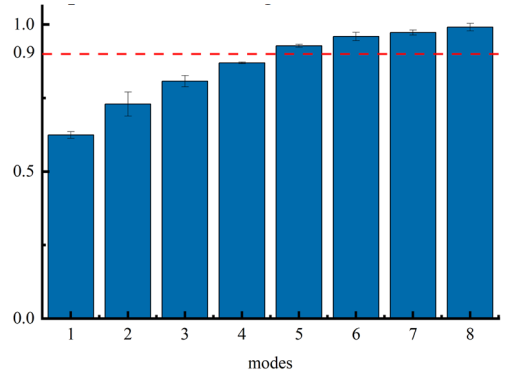

Fig. 2. Muscle synergies extracted from sEMG envelopes. Five components were required to explain 90% of the variance.

variables. The significance level was set at 0.05 ($\alpha = 0.05$). The Brain Connectivity Toolbox was used to calculate all the above network metrics [29].

III. Results

A. Muscle Synergy

Five muscle synergies were identified from the original sEMG envelope under gait motion. The five muscle synergies accumulated to 90% of the Frobenius norm of the original sEMG envelope, as shown in Fig. 2.

More detailed results presented in Fig. 3 indicate five synergistic modes. In those observed in the low-speed group (Fig.3A), synergistic modes 1 and 4 consisted mainly of TA and VM, respectively, rather than a combination of muscles. Synergistic mode 2 consisted mainly of TA, GM, and SO. Synergistic mode 3 consisted primarily of ST and BF. Synergistic mode 5 consisted mainly of RF and VL. The results in the medium-speed group depicted in Fig.3B were similar to those in the low-speed group, with smaller variations in individual synergistic patterns. The muscle synergy restructuring was observed in the high-speed group (Fig.3C). A different muscle synergy pattern from the low- and medium-speed groups appeared, with the disappearance of synergy pattern 4 (with VM as the primary contributor) and synergy pattern 5 (with RF and VL as the main contributors), being replaced by two new muscle synergy patterns with RF+VM and VL as the main contributors, respectively.

B. Functional Muscle Networks

Ninety percent of the global VAF was used to determine the number of functional muscle networks. The coherence spectrum was decomposed into two patterns that reflected different frequency bands (0-25 Hz and 25-50 Hz), i.e., different functional muscle connections exhibited in two different frequency ranges, as shown in Fig. 4 (identified by NNMF from low to high frequencies).

Figures 5, 6, and 7 show the functional muscle networks for the low-, medium-, and high-speed groups, respectively. The left column shows two undirected weighted adjacency matrices (8×8). The topographies of the functional muscle networks in the right column correspond to the respective spectral coherence patterns and adjacency matrices. The thickness of the connecting lines of the network topographies correspond to the sizes of the related elements in the adjacency matrices.

At the three different gait speed levels, despite the same numbers of functional muscle networks in each group, there were variations within the networks caused by differences in speed. During the low-frequency component interval, the undirected adjacency matrix between the medium- and high-speed groups had significantly larger weights than the low-speed group. In the low-speed condition, the connectivity of RF and VL muscles is low, the connectivity of VM and SO muscles is low, the connectivity of VL and SO muscles is low, which increases in the medium-speed mode, and the connectivity of VM and VL muscles is low in the medium-speed mode, which increases in the high-speed mode. In the high-frequency component interval, the coupling strength between muscles changed with increasing speed. The coupling degree between GM and SO muscles varied significantly between the low-, medium-, and high-speed groups, it shows an increase in the coupling strength between GM and SO muscles as the gait speed increases. The RF and VL muscles showed lower connectivity in the low-speed condition, which increased in the medium-speed mode. The coupling strength of the ST and BF muscles was closer under the low- and medium-speed conditions, and the coupling became stronger under the high-speed conditions. The edge weights of the functional muscle network topographies were plotted according to the strength of connectivity as low strength (thin dashed line), medium strength (thin solid line), and high strength (thick solid line), proportional to the maximum edge weight of each group.

C. Complex Network Analysis

To quantify the internal connections of the functional muscle networks, three network metrics were calculated: global efficiency, clustering coefficient, and betweenness centrality (Fig. 8). The global efficiency and clustering coefficients of the network differed significantly under various speed conditions reaching $F(2,15)=6.607$, $p = 0.009$ versus $F(2,15)=7.883$, $p = 0.005$. The *post hoc* tests revealed that the global efficiencies in low- and high-speed conditions differed in the low-frequency band (0-25 Hz), reaching $p = 0.048$. In the high-frequency band (25-50 Hz), they exhibited a significant difference between low- and medium-speed conditions ($p = 0.012$), as well as between low- and high-speed conditions ($p = 0.004$). The clustering coefficients showed a significant difference ($p = 0.037$) between the low- and high-speed conditions in the low-frequency band (0-25 Hz). In the high-frequency band (25-50 Hz), there was a significant difference ($p = 0.004$) between the low- and medium-speed conditions, as well as a significant difference ($p = 0.004$) between the low- and high-speed conditions. The network's global efficiency and clustering coefficients tended to become larger and smaller as the speed increased. However, this was not reflected in the betweenness centrality metric. Meanwhile, higher frequency ranges featured lower global efficiencies and clustering coefficients.

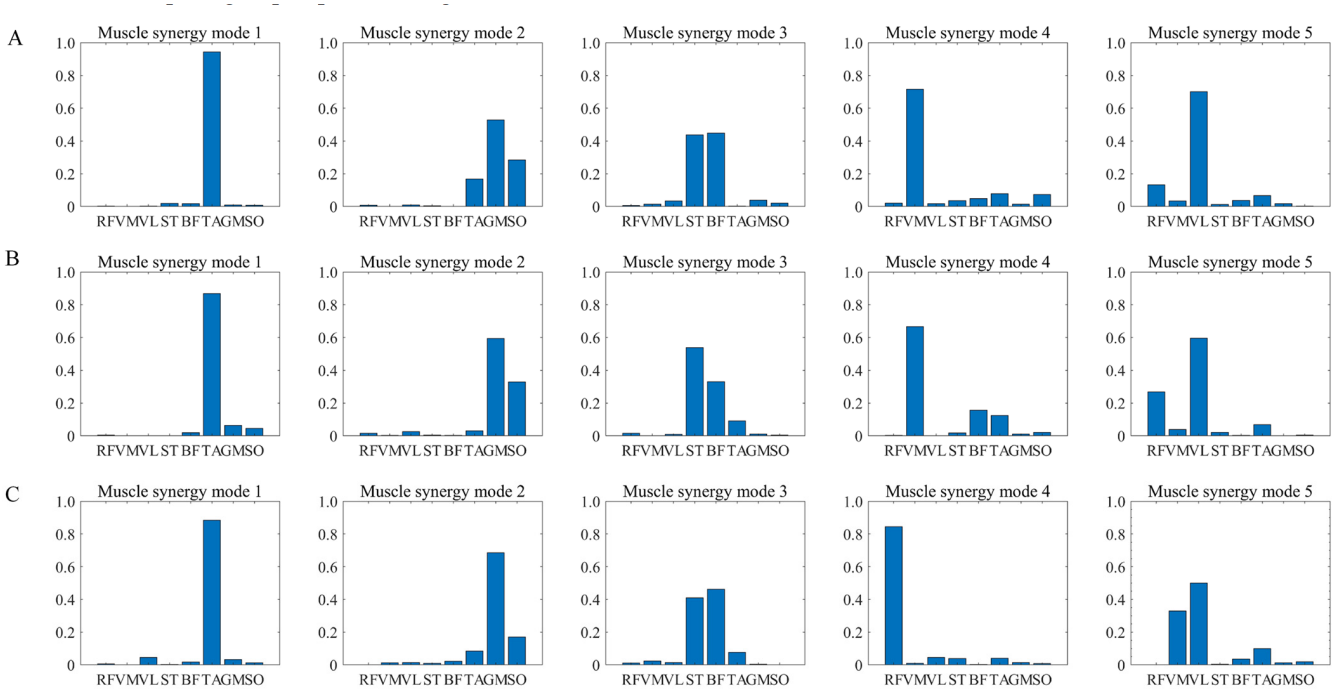

Fig. 3. Muscle synergies extracted using nonnegative matrix factorization. (A) Synergetic effect of eight muscles in the low-speed group. (B) Synergetic effect of eight muscles in the medium-speed group. (C) Synergistic effect of eight muscles in the high-speed group.

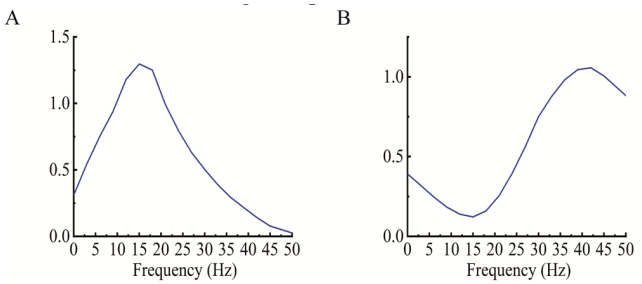

Fig. 4. Frequency components obtained by nonnegative matrix factorization. (A) Low-frequency component (0-25 Hz). (B) High-frequency component (25-50 Hz).

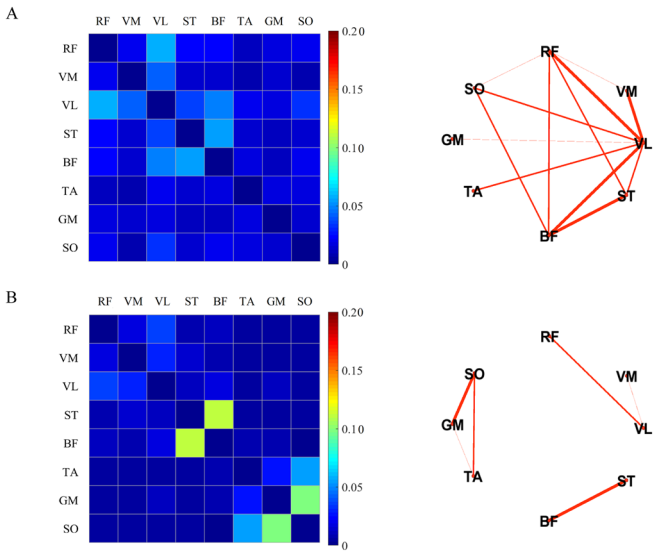

Fig. 5. The functional muscle networks of the low-speed group: (A) the functional muscle networks of the low-frequency component (0-25 Hz) are shown in the left column and the corresponding network topology in the right column; (B) The left column shows the functional muscle networks of the high-frequency component (25-50 Hz), and the right column shows the corresponding network topology.

IV. Discussion

Insofar as synergy is essential for human motor control in simple daily gait tasks, this study combines the construction of the functional muscle network with muscle synergy analysis to grasp the changes in muscle connectivity at different gait speeds in adult male participants. Their lower limb sEMG signals were collected under three different gait speed conditions to extract muscle synergies and construct functional muscle networks. We extracted five muscle synergies in human gait motion, consistent with previous studies [30]. As the speed of gait movement increased, the corresponding restructuring of muscle synergy was observed, especially between the medium- and high-speed groups. The muscle synergy restructuring reflected electromyographic activity modulation [31].

In the muscle synergy model 2 with GM and SO as the main contributors, the contribution of GM increases with increasing gait speed, while the contribution of SO decreases with increasing gait speed. One possible reason for this phenomenon is that in humans, there are both fast and slow muscle fibers in the same muscle. However, the distribution ratio of fast muscle fibers and slow muscle fibers in different muscles is different. The GM has a higher component of fast muscle fibers and plays a significant role in strenuous movements such as high-speed running, jumping, etc., while

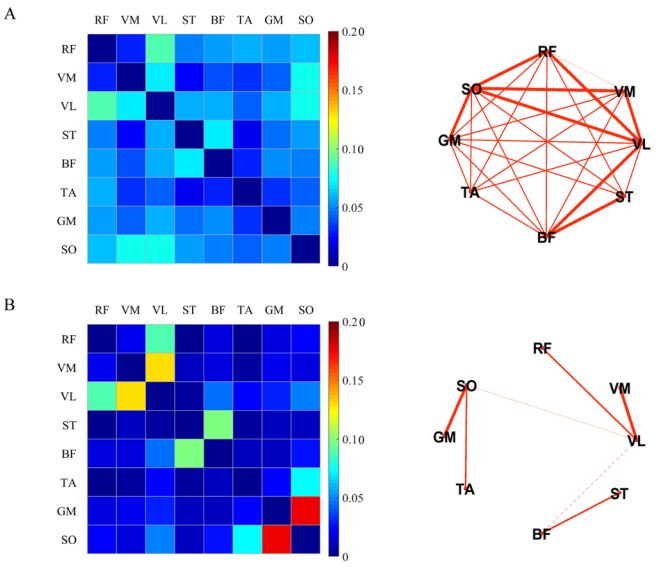

Fig. 6. The functional muscle networks of the medium-speed group. (A) The left column shows the functional muscle networks of the low-frequency component (0-25 Hz), and the right column shows the corresponding network topology. (B) The left column shows the functional muscle networks of the high-frequency component (25-50 Hz), and the right column shows the corresponding network topology.

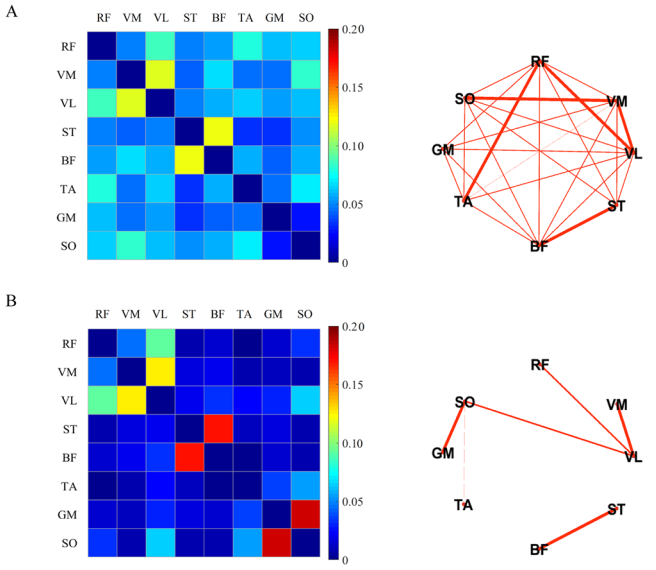

Fig. 7. The functional muscle networks of the high-speed group. (A) The left column shows the functional muscle networks of the low-frequency component (0-25 Hz), and the right column shows the corresponding network topology. (B) The left column shows the functional muscle networks of the high-frequency component (25-50 Hz), and the right column shows the corresponding network topology.

the SO has a higher component of slow muscle fibers and plays a significant role in movements such as walking and jogging [32], [33].

Muscle functional connectivity showed different modulations in subjects at various gait speeds, with increased functional connectivity between ST and BF and GM and SO in lower limb muscles with increasing speed. This implied

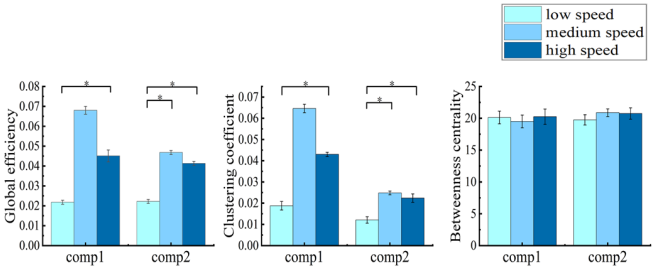

Fig. 8. Global efficiency, clustering coefficient, and betweenness centrality of the coherence networks per frequency component (comp1=0–25 Hz, comp2=25–50 Hz) and condition. Error bars indicate standard errors of the mean, and asterisks indicate significant differences between conditions ($p < 0.05$).

that functional connectivity between muscles during gait tasks in humans was influenced by motion speed, i.e., the faster the gait motion, the stronger the coupling between lower limb muscles, which may be the result of intermuscular coherence in healthy subjects modulating according to the difficulty of the movement task [34]. This also demonstrated the existence of multifunctional circuits, i.e., the ability to produce different control schemes under different conditions within a fixed pattern of muscle anatomical connections in the human body [35]. Such circuits create the basis to support increasingly complex behaviors driven by multiple circuits acting in concert rather than a single, direct pathway. Some neural patterns may limit the potential functional connectivity of skeletal muscles [36].

The effect of gait speed changes on the functional muscle networks manifests in different frequency ranges, suggesting the multiplex network functionality. Various frequency components correspond to varying levels of muscle function connectivity. In particular, nonnegative matrix decomposition extracted two different frequency components: 0-25 Hz and 25-50 Hz. These two components may reflect the spectral patterns of different pathways projecting to spinal motor neurons. The unique topology of the cross-frequency functional muscle networks suggests that different pathways support common inputs in various frequency bands. These different frequencies may play specific roles in encoding motor signals. The lowest-frequency component of functional muscle connectivity may be derived from the afferent pathway. The higher-frequency component of functional muscle connectivity may reflect relevant inputs from the downstream pathway [37]. It can be speculated that the central nervous system is composed of multiple unique neural circuits, each responsible for the co-modulation of certain muscles in a specific frequency range. Although this study did not directly assess the connections between the cerebral cortex and muscles, it interpreted the different frequency ranges as distinct neural pathways that might reflect afferent and efferent inputs to spinal motor neurons, respectively [38]. A previous study showed that functional connectivity in the beta band most likely reflected corticospinal mapping [39].

This study found more localized functional connectivity at low-, medium-, and high-speed gait conditions in the higher

frequency components, which were sparser in the network topology map. This more localized connectivity pattern may reflect the propriospinal pathway [40]. This is consistent with previous studies of cortical networks, where lower-frequency ranges reflected more extensive coupling, while higher-frequency ranges reflected local coupling [41]. The brain's control of muscles is not simply one-to-one control but many-to-many modular control [42]. The brain controls synergy between muscles during gait movements to simplify control strategies.

The current study revealed that the synergistic muscles observed in the muscle synergy analysis corresponded to the muscle combinations with high coupling strength in the constructed functional muscle networks. The muscle synergy analysis revealed more substantial contributions from GM to SO and ST to BF and the higher coupling strength between GM and SO and ST and BF in the functional muscle networks. This suggests that muscle synergy corresponds to functional muscle networks, consistent with previous findings that muscle synergy can be mapped into functional muscle networks. The latter provides graphical information on muscle synergy for inferring an understanding of functional connections between muscles [43]. The muscle synergy analysis extracted motor modules with synergistic relationships, and the functional muscle networks quantitatively analyzed the coupling relationship between synergistic and non-synergistic muscle pairs. From the effective combination of both central neural control of motor patterns and neural information transmission for motor function evaluation.

In this study, we combined the muscle synergy analysis with constructing functional muscle networks to investigate the mechanisms of action of human lower limb muscles at different gait speeds, including coordination between muscles and the neural realization of muscle synergy. This study did not directly assess the contributions from supraspinal inputs; other directed information-theoretic measures were used to determine these inputs [44]. Zandvoort et al. discussed the contribution of the cortex to synergy formation by combining electroencephalogram (EEG) with sEMG-based synergy analysis [45]. The study by Artoni et al. showed that the human motor cortex actively controls contralateral leg muscles during walking, demonstrating a unidirectional brain-muscle connection between proximal and distal muscles, and that lower limb muscles are "finely" controlled during stereotypic movements on a treadmill through a network of areas in the motor cortex known to be involved in nonstationary standing movements (e.g., precise stepping) and motor planning [46]. In the follow-up study, network analysis will assess functional interactions between the brain, spinal cord, and skeletal muscles. This approach may open up new perspectives for treating neurological diseases.

This study has certain limitations. First, only young participants were recruited in this study. Aging has been shown to affect the body's motor system, and the difference in the mechanism of lower limb muscle action between different age groups is not clear. Secondly, only male participants were recruited in this study, and the effect of gender differences on gait movement was not considered, although there are currently no consistent data showing convincing differences in the sEMG responses of men and women during gait movement, we may find more differences in the future. In the future, based on the current research, we will further explore the muscle coordination and functional muscle network differences in gait movement between different populations.

V. Conclusion

Combining muscle synergy analysis with the construction of functional muscle networks to study lower limb muscles in humans under different gait speed conditions, we identified a restructuring of muscle synergy, exhibiting functional connections between multiple muscle groups at different frequencies. The unique topology of the functional muscle networks across frequencies indicated that different pathways supported common inputs in various frequency bands. The functional network in all muscle pairs was more localized between muscles in the high-frequency range, suggesting a stronger functional connection between muscles.

References

[1] J. L. Lelas, G. J. Merriman, P. O. Riley, and D. C. Kerrigan, "Predicting peak kinematic and kinetic parameters from gait speed," *Gait Posture*, vol. 17, no. 2, pp. 106–112, 2003.

[2] M. Inzitari et al., "Gait speed predicts decline in attention and psychomotor speed in older adults: The health aging and body composition study," *Neuroepidemiology*, vol. 29, nos. 3–4, pp. 156–162, 2007.

[3] J. Afilalo et al., "Gait speed as an incremental predictor of mortality and major morbidity in elderly patients undergoing cardiac surgery," *J. Amer. College Cardiol.*, vol. 56, no. 20, pp. 1668–1676, Nov. 2010.

[4] B. R. Schlink, A. D. Nordin, and D. P. Ferris, "Human myoelectric spatial patterns differ among lower limb muscles and locomotion speeds," *Physiolog. Rep.*, vol. 8, no. 23, Dec. 2020, Art. no. e14652.

[5] A. L. Hof, H. Elzinga, W. Grimmius, and J. P. K. Halbertsma, "Speed dependence of averaged EMG profiles in walking," *Gait Posture*, vol. 16, no. 1, pp. 78–86, Aug. 2002.

[6] E. M. McCain et al., "Mechanics and energetics of post-stroke walking aided by a powered ankle exoskeleton with speed-adaptive myoelectric control," *J. Neuroeng. Rehabil.*, vol. 16, no. 1, pp. 1–12, 2019.

[7] C. A. Byrne, D. T. O'Keeffe, A. E. Donnelly, and G. M. Lyons, "Effect of walking speed changes on tibialis anterior EMG during healthy gait for FES envelope design in drop foot correction," *J. Electromyogr. Kinesiol.*, vol. 17, no. 5, pp. 605–616, Oct. 2007.

[8] R. E. A. Van Emmerik and R. C. Wagenaar, "Effects of walking velocity on relative phase dynamics in the trunk in human walking," *J. Biomech.*, vol. 29, no. 9, pp. 1175–1184, Sep. 1996.

[9] A. d'Avella, P. Saltiel, and E. Bizzi, "Combinations of muscle synergies in the construction of a natural motor behavior," *Nature Neurosci.*, vol. 6, pp. 300–308, Mar. 2003.

[10] V. C. K. Cheung, A. d'Avella, M. C. Tresch, and E. Bizzi, "Central and sensory contributions to the activation and organization of muscle synergies during natural motor behaviors," *J. Neurosci.*, vol. 25, pp. 6419–6434, Jul. 2005.

[11] F. D. Groote, I. Jonkers, and J. Duysens, "Task constraints and minimization of muscle effort result in a small number of muscle synergies during gait," *Frontiers Comput. Neurosci.*, vol. 8, p. 115, Sep. 2014.

[12] B. Pan et al., "Alterations of muscle synergies during voluntary arm reaching movement in subacute stroke survivors at different levels of impairment," *Frontiers Comput. Neurosci.*, vol. 12, p. 69, Aug. 2018.

[13] D. J. Clark, L. H. Ting, F. E. Zajac, R. R. Neptune, and S. A. Kautz, "Merging of healthy motor modules predicts reduced locomotor performance and muscle coordination complexity post-stroke," *J. Neurophys.*, vol. 103, no. 2, pp. 844–857, Dec. 2009.

[14] G. Buzsaki, *Rhythms of the Brain*. New York, NY, USA: Oxford Univ. Press, 2006.

[15] T. Liang et al., "Directed network analysis reveals changes in cortical and muscular connectivity caused by different standing balance tasks," *J. Neural Eng.*, vol. 19, no. 4, Jul. 2022, Art. no. 046021.

[16] X. Zhang et al., "Correlation analysis of EEG brain network with modulated acoustic stimulation for chronic tinnitus patients," *IEEE Trans. Neural Syst. Rehabil. Eng.*, vol. 29, pp. 156–162, 2021.

[17] S. Mehrkanoon, M. Breakspear, and T. W. Boonstra, "The reorganization of corticomuscular coherence during a transition between sensorimotor states," *NeuroImage*, vol. 100, pp. 692–702, Oct. 2014.

[18] D. M. Halliday and J. R. Rosenberg, "On the application, estimation and interpretation of coherence and pooled coherence," *J. Neurosci. Methods*, vol. 100, nos. 1–2, pp. 173–174, Jul. 2000.

[19] J. N. Kerkman, A. Daffertshofer, L. L. Gollo, M. Breakspear, and T. W. Boonstra, "Functional connectivity analysis of multiplex muscle network across frequencies," in *Proc. 39th Annu. Int. Conf. IEEE Eng. Med. Biol. Soc.*, Jul. 2017, pp. 1567–1570.

[20] M. Houston, X. Li, P. Zhou, S. Li, J. Roh, and Y. Zhang, "Alterations in muscle networks in the upper extremity of chronic stroke survivors," *IEEE Trans. Neural Syst. Rehabil. Eng.*, vol. 29, pp. 1026–1034, 2021.

[21] L. Xu et al., "Motor execution and motor imagery: A comparison of functional connectivity patterns based on graph theory," *Neuroscience*, vol. 261, pp. 184–194, Mar. 2014.

[22] E. Piovanelli et al., "Towards a simplified estimation of muscle activation pattern from MRI and EMG using electrical network and graph theory," *Sensors*, vol. 20, no. 3, p. 724, Jan. 2020.

[23] X. Xi, S. Pi, Y.-B. Zhao, H. Wang, and Z. Luo, "Effect of muscle fatigue on the cortical-muscle network: A combined electroencephalogram and electromyogram study," *Brain Res.*, vol. 1752, Feb. 2021, Art. no. 147221.

[24] M. Tresch, V. Cheung, and A. D'Avella, "Matrix factorization algorithms for the identification of muscle synergies: Evaluation on simulated and experimental data sets," *J. Neurophys.*, vol. 95, no. 4, pp. 2199–2212, Apr. 2005.

[25] L. H. Ting and J. M. Macpherson, "A limited set of muscle synergies for force control during a postural task," *J. Neurophys.*, vol. 93, no. 1, pp. 609–613, 2005.

[26] T. Wojtara, F. Alnajjar, S. Shimoda, and H. Kimura, "Muscle synergy stability and human balance maintenance," *J. Neuroeng. Rehabil.*, vol. 11, no. 1, pp. 1–9, 2014.

[27] E. Bullmore and O. Sporns, "Complex brain networks: Graph theoretical analysis of structural and functional systems," *Nature Rev. Neurosci.*, vol. 10, no. 3, pp. 186–198, Mar. 2009.

[28] D. J. Watts and S. H. Strogatz, "Collective dynamics of 'small-world' networks," *Nature*, vol. 393, nos. 66–84, pp. 440–442, 1998.

[29] M. Rubinov and O. Sporns, "Complex network measures of brain connectivity: Uses and interpretations," *NeuroImage*, vol. 52, no. 3, pp. 1059–1069, 2010.

[30] Y. P. Ivanenko, R. E. Poppele, and F. Lacquaniti, "Five basic muscle activation patterns account for muscle activity during human locomotion," *J. Physiol.*, vol. 556, no. 1, pp. 267–282, 2004.

[31] J. N. Kerkman, A. Bekius, T. W. Boonstra, A. Daffertshofer, and N. Dominici, "Muscle synergies and coherence networks reflect different modes of coordination during walking," *Frontiers Physiol.*, vol. 11, p. 751, Jul. 2020.

[32] A. Lai, G. A. Lichtwark, A. G. Schache, Y. C. Lin, and M. G. Pandy, "In vivo behavior of the human soleus muscle with increasing walking and running speeds," *J. Appl. Physiol.*, vol. 118, no. 10, pp. 1266–1275, 2015.

[33] P. D. Gollnick, B. Sjodin, J. Karlsson, E. Jansson, and B. Saltin, "Human soleus muscle: A comparison of fiber composition and enzyme activities with other leg muscles," *Pflügers Arch. Eur. J. Physiol.*, vol. 348, no. 3, pp. 247–255, 1974.

[34] A. Oshima, T. Wakahara, Y. Nakamura, N. Tsujiuchi, and K. Kamibayashi, "Time-series changes in intramuscular coherence associated with split-belt treadmill adaptation in humans," *Exp. Brain Res.*, vol. 239, no. 7, pp. 2127–2139, Jul. 2021.

[35] K. L. Briggman and W. B. Kristan, "Multifunctional pattern-generating circuits," *Annu. Rev. Neurosci.*, vol. 31, no. 1, pp. 271–294, Jul. 2008.

[36] J. A. Gallego, M. G. Perich, L. E. Miller, and S. A. Solla, "Neural manifolds for the control of movement," *Neuron*, vol. 94, no. 5, pp. 978–984, 2017.

[37] J. N. Kerkman, A. Daffertshofer, L. L. Gollo, M. Breakspear, and T. W. Boonstra, "Network structure of the human musculoskeletal system shapes neural interactions on multiple time scales," *Sci. Adv.*, vol. 4, no. 6, Jun. 2018, Art. no. eaat0497.

[38] M. Bourguignon, V. Jousmäki, S. S. Dalal, K. Jerbi, and X. De Tiège, "Coupling between human brain activity and body movements: Insights from non-invasive electromagnetic recordings," *NeuroImage*, vol. 203, Dec. 2019, Art. no. 116177.

[39] I. E. J. de Vries, A. Daffertshofer, D. F. Stegeman, and T. W. Boonstra, "Functional connectivity in the neuromuscular system underlying bimanual coordination," *J. Neurophys.*, vol. 116, no. 6, pp. 2576–2585, Dec. 2016.

[40] E. Pierrot-Deseilligny and D. Burke, *The Circuitry of the Human Spinal Cord: Its Role in Motor Control and Movement Disorders*. Cambridge, U.K.: Cambridge Univ. Press, 2005.

[41] O. Sporns, D. R. Chialvo, M. Kaiser, and C. C. Hilgetag, "Organization, development and function of complex brain networks," *Trends Cogn. Sci.*, vol. 8, no. 9, pp. 418–425, Sep. 2004.

[42] M. Graziano, "The organization of behavioral repertoire in motor cortex," *Annu. Rev. Neurosci.*, vol. 29, no. 1, pp. 105–134, Jul. 2006.

[43] A. Bashan, R. P. Bartsch, J. W. Kantelhardt, S. Havlin, and P. C. Ivanov, "Network physiology reveals relations between network topology and physiological function," *Nature Commun.*, vol. 3, no. 1, pp. 1–9, Feb. 2012.

[44] T. W. Boonstra, L. Faes, J. N. Kerkman, and D. Marinazzo, "Information decomposition of multichannel EMG to map functional interactions in the distributed motor system," *NeuroImage*, vol. 202, Nov. 2019, Art. no. 116093.

[45] C. S. Zandvoort, J. H. van Dieen, N. Dominici, and A. Daffertshofer, "The human sensorimotor cortex fosters muscle synergies through cortico-synergy coherence," *NeuroImage*, vol. 199, pp. 30–37, Oct. 2019.

[46] F. Artoni et al., "Unidirectional brain to muscle connectivity reveals motor cortex control of leg muscles during stereotyped walking," *NeuroImage*, vol. 159, pp. 403–416, Oct. 2017.